Available online at www.sciencedirect.com

ScienceDirect

Advances in Space Research 71 (2023) 2521–2533

ADVANCES IN SPACE RESEARCH (a COSPAR publication)

www.elsevier.com/locate/asr

Relationships between energetic storm particle events and interplanetary shocks driven by full and partial halo coronal mass ejections

Dheyaa Ameri [a,*,1], Eino Valtonen [b], Amjad Al-Sawad [c], Rami Vainio [d]

[a] Department of Ecology, University of Basrah, Karmat Ali B.P. 49, Basrah, Iraq
[b] Department of Physics and Astronomy, University of Turku, 20014 Turku, Finland
[c] Ministry of Higher Education and Scientific Research, Baghdad, Iraq
[d] Department of Physics and Astronomy, University of Turku, 20014 Turku, Finland

Received 30 May 2022; received in revised form 28 November 2022; accepted 6 December 2022
Available online 13 December 2022

Abstract

We have analysed energetic storm particle (ESP) events in 116 interplanetary (IP) shocks driven by front-side full and partial halo coronal mass ejections (CMEs) with speeds >400 km s^{-1}during the years 1996–2015. We investigated the occurrence and relationships of ESP events with several parameters describing the IP shocks, and the associated CMEs, type II radio bursts, and solar energetic particle (SEP) events. Most of the shocks (57%) were associated with an ESP event at proton energies >1 MeV.

The shock transit speeds from the Sun to 1 AU of the shocks associated with an ESP event were significantly greater than those of the shocks without an ESP event, and best distinguished these two groups of shocks from each other. The occurrence and maximum intensity of the ESP events also had the strongest dependence on the shock transit speed compared to the other parameters investigated. The correlation coefficient between ESP peak intensities and shock transit speeds was highest (0.73 ± 0.04) at 6.2 MeV. Weaker dependences were found on the shock speed at 1 AU, Alfvénic and magnetosonic Mach numbers, shock compression ratio, and CME speed. On average all these parameters were significantly different for shocks capable to accelerate ESPs compared to shocks not associated with ESPs, while the differences in the shock normal angle and in the width and longitude of the CMEs were insignificant.

The CME-driven shocks producing energetic decametric–hectometric (DH) type II radio bursts and high-intensity SEP events proved to produce also more frequently ESP events with larger particle flux enhancements than other shocks. Together with the shock transit speed, the characteristics of solar DH type II radio bursts and SEP events play an important role in the occurrence and maximum intensity of ESP events at 1 AU.

Keywords: Energetic particles; Solar particles; Energetic storm particles; Coronal mass ejections; Type II radio bursts; Interplanetary shocks

1. Introduction

Energetic storm particle (ESP) events are defined as enhancements in energetic ion and electron intensities observed during an interplanetary (IP) shock passage (Bryant et al., 1962; Rao et al., 1967). IP shocks are primarily driven by coronal mass ejections (CMEs) and their interplanetary counterparts (ICMEs) (e.g., Lindsay et al.

* Corresponding author.
E-mail addresses: dheyaa.abdulsada@uobasrah.edu.iq (D. Ameri), eino.valtonen@utu.fi (E. Valtonen), dr.amjad@scrdiraq.gov.iq (A. Al-Sawad), rami.vainio@utu.fi (R. Vainio).
[1] Also at Department of Physics and Astronomy, University of Turku, 20014 Turku, Finland.

https://doi.org/10.1016/j.asr.2022.12.014
0273-1177/

(1994); Berdichevsky et al. (2000)) and sometimes by stream interaction regions (e.g., Jian et al. (2006) and references therein).

The time-intensity profiles of ESP events differ from event to event. Two categories of ESP events based on the observed particle intensities were proposed by Sarris and Van Allen (1974): spike events and classic events. In spike events, the time profiles show a rapid change in particle intensities. The maximum energy at which the proton intensity increases is rarely observed to exceed 5 MeV. These events are a result of the shock drift acceleration at quasi-perpendicular shocks. In classic events, the time-intensity profiles of particles change gradually. These events can last for several hours and particles may arrive ahead or behind the shock. The maximum energy at which the proton increases are observed in classical events is higher than in spike events, extending to well above ~20 MeV. The source of the classic ESP events is diffusive shock acceleration at quasi-parallel shocks (e.g., see Tsurutani and Lin (1985); Kallenrode (1995); Lario et al. (2003); Lario et al. (2005); Ho et al. (2003); Cohen (2006)).

Many studies have investigated the characteristics of ESP events and their dependence on the solar sources and shock parameters. Ho et al. (2008) investigated the occurrence of ESP events for a large sample of IP shocks in solar cycle 23 based on the EPAM instrument onboard the Advanced Composition Explorer (ACE) spacecraft. They found ion flux enhancements in the 47–68 keV and 1.9–4.8 MeV energy ranges in 64% and 32% of the shocks, respectively, and 20% of the shocks were associated with an electron flux enhancement in the 38–53 keV energy range. In a statistical analysis of SEP events during solar cycle 23, Dierckxsens et al. (2015) collected a list of 90 SEP events in the proton energy range 7.23–10.45 MeV, which were associated with solar flares of at least magnitude M1. In 45 (50%) of these events an ESP component was identified, associated with a shock at 1 AU. Giacalone (2012) found that all strong interplanetary shocks (with compression ratio >2.5 and Alfvénic Mach number >3) observed by ACE in 1998–2003 were able to accelerate protons up to energies 47–65 keV. Lario et al. (2005) studied the characteristics of ESP signatures for 191 fast forward transient shocks observed by the ACE spacecraft. They showed that more energetic shocks have greater effects on local particle fluxes, but the characteristics of the ESP events were not strongly dependent on the shock parameters. In a statistical study of ESP events observed by SOHO/ERNE above 1.5 MeV, Huttunen-Heikinmaa and Valtonen (2009) found that the ESP events were observed in only 40% of the fast forward shocks. They also showed that the high-energy ESP-effectiveness of the fast forward shocks had a solar cycle dependence with the yearly effectiveness being about five times higher during solar maximum compared to minimum.

Mäkelä et al. (2011) investigated the occurrence and characteristics of ESP events associated with shocks driven by CMEs. They found that the CMEs were significantly more energetic and Alfvénic Mach numbers significantly higher in the CME-driven shocks producing ESP events compared to those without an ESP event. They also observed that the ESP events occurred more frequently and had higher intensities in the shocks with radio type II bursts in the metric-to-kilometric wavelength range compared to shocks without these type II bursts, and that the maximum intensities of ESP events showed strong positive correlations with the CME speeds and the shock speeds at 1 AU. In the study of significant in situ shock acceleration of He ions of 1–10 MeV at 258 IP shocks observed by the Wind spacecraft, Reames (2012) showed that the probability of a significant acceleration and ESP peak intensity were strongly dependent on the shock speed and weakly dependent on the shock compression ratio, while there was no dependence between the ESP peak intensity and the shock-normal angle. Ebert et al. (2016) studied the fluxes of 0.1–20 MeV O and Fe ions during seven multi-spacecraft ESP events and the associated IP shock properties at 1 AU. They showed that the O and Fe time-intensity profiles varied significantly between longitudinally separated spacecraft observing the same event, and that the O and Fe peak intensities had weak to no correlations with the shock parameters. In a recent study Dayeh et al. (2018) investigated the relations between the ESP characteristics and both IP shock and IP CME (ICME) properties. They concluded that spectral and compositional relations strongly supported a rigidity-dependent acceleration mechanism. The shock speed and ICME sheath temperature showed moderate to poor correlations with the ESP characteristics.

High-energy particle radiation in space is a significant constituent of space weather. Temporal changes in near-Earth radiation environment are a major concern due to the presence of humans in space and increasing sensitivity of space flight equipment to radiation (Cohen, 2006). Unexpected occurrence of ESP events can cause sudden, orders of magnitude increases of particle intensities (see e.g., Reames (1999); Reames (2004); Turner (2001), Cohen (2006)). Our investigation aims to finding signatures in various environmental parameters associated with ESP events that could be used as warning signals of strong ESP events.

In this article we investigate ESP events at proton energies >1 MeV associated with the passage of IP shocks driven by front-side full and partial halo CMEs with speeds >400 km s^{-1}. The selection of data is described in Section 2. The statistics of the selected IP shocks and the associated ESP events are presented in Section 3.1. The characteristics of the IP shocks and their associations with solar events for shocks with and without an ESP event are discussed in Section 3.2. The correlation analysis of the maximum intensities of the ESP events with the shock parameters and the properties of the associated CMEs and solar energetic particle (SEP) events at the Sun are carried out in Section 3.3. The results are summarized and discussed in Section 4. Conclusions in Section 5 complete the article.

2. Data sources and event selection

The CME catalog of the SOHO Large Angle Spectroscopic Coronagraph (LASCO) (Brueckner et al., 1995) at https://cdaw.gsfc.nasa.gov/CME_list/ was used to select the CMEs. To identify the solar locations of the CMEs we assume the CME launch sites to coincide with the locations of the associated GOES soft X-ray flares given at https://hesperia.gsfc.nasa.gov/goes/goes_event_listings/. For this investigation we selected full and partial (angular width >120°) halo CMEs with speeds >400 km s^{-1}launched from the front side of the Sun during the period from the beginning of 1996 to the end of 2015. For CME widths and speeds we use the sky-plane widths and linear speeds as given in the LASCO CME catalog.

The occurrence times and characteristics of the IP shocks that we associated with the selected CMEs were obtained from the online IP shock database of the Wind and ACE spacecraft (https://lweb.cfa.harvard.edu/shocks/). In this database, the shock parameters are estimated by using eight different methods as described by Kasper (2003). The median value and the standard deviation of those eight methods were used in the analysis as the shock parameters and their uncertainties, respectively. For a few events we discarded clearly unphysical results from the median and its standard deviation. The shock speed (V_{sh}), Alfvénic Mach number (M_A), magentosonic Mach number (M_{ms}), compression ratio (CR_{sh}), and shock normal angle (θ_{bn}) were used in our investigation. Alfvénic and magnetosonic Mach numbers were calculated by using the formulas $M_A = V_{up}/V_A$ and $M_{ms} = V_{up}/\sqrt{V_A^2 + V_s^2}$(e.g., Lario et al. (2005); Edberg et al. (2010)). The upstream plasma speed (V_{up}), the Alfvén speed (V_A), and the sound speed (V_s) were obtained from the IP shock database.

For associating CMEs with IP shocks we estimated the arrival time at 1 AU of an ICME corresponding to an observed CME by using the drag-based model of Vršnak et al. (2013). If the observed IP shock time was within a ±24 h time window from the predicted arrival time of the ICME, the related CME was associated with the IP shock. If the IP shock time occurred within the arrival time windows of several ICMEs, the CME with the closest arrival time to the shock time was assumed to be the source of the shock. If more than one shock was seen within the arrival time windows, the CME-shock couples were chosen based on their temporal sequence. We also used the list of CME-driven shocks observed at 1 AU from Gopalswamy et al. (2010a) and the online catalog of SOHO/CELIAS (http://umtof.umd.edu/pm/) to assist associating CMEs with IP shocks at 1 AU.

For searching the energetic particle events related to the CME-driven shocks we used the European Space Agency (ESA) Solar Energetic Particle Environment Modelling (SEPEM) database (http://www.sepem.eu/) (Crosby et al., 2015). The cleaning of the datasets derived from the many GOES missions has been carried out in this project. For more details about the features of the SEPEM server see Crosby et al. (2015). The SEPEM Reference Data Set (version 2.01) has eleven energy channels extending from 5–7.2 MeV (nominal energy 6.2 MeV) to 200–289 MeV (248 MeV). We also used the proton measurements of the Energetic and Relativistic Nuclei and Electron experiment (ERNE) (Torsti et al., 1995) aboard the Solar and Heliospheric Observatory (SOHO) spacecraft. The SOHO/ERNE has two detectors, low and high energy detectors, covering an energy range from 1.58 MeV to 131 MeV. We define an ESP event as an increase of particle intensity at the shock passage at least 20% above the observed background intensity. The ESP peak intensity often occurred within a ±2 h time window from the observed shock time. The background intensity was estimated during a time period before the start of the ESP event (see, Mäkelä et al. (2011); Reames (2012)). Thus, the background was either the intensity of the ongoing SEP event before the start of the ESP event or the quiet-time particle intensity. Most of the ESP events were preceded by SEP events. To record an SEP event, the particle intensity should increase by a factor of 3 above the pre-event background intensity within a few hours (<3 h) after the launch of the CME (e.g., Kouloumvakos et al. (2015)). The corrected ESP peak intensity was estimated by subtracting the background from the observed total intensity. Fig. 1 shows the time-intensity profile of the energetic particle event on July 25, 2004 provided by the SEPEM server at four energy ranges.

We used the online catalogs provided by the Wind and STEREO data center (https://solar-radio.gsfc.nasa.gov/winddata_products.html) for decametric–hectometric (DH) type II bursts and Solar Geophysical Data (SGD) for metric (m) type II bursts to associate solar type II radio bursts with the events. For event dates with no reported m type II bursts in SGD, we further checked the radio dynamic spectra provided by Hiraiso Radio Spectrograph (HiRAS), the Radio Solar Telescope Network (RSTN), Bruny Island Radio Spectrometer (BIRS), Green Bank Solar Radio Burst Spectrometer (GBSRBS), and Nancay Decameter Array (NDA).

3. Data analysis

3.1. Statistics

The starting point of the study was front-side full and partial halo CMEs with speeds >400 km s^{-1}from the LASCO catalog. All CMEs fulfilling our selection criteria (see Section 2) and and followed within 1 to 4 days after launch by an IP shock at 1 AU were selected for further investigation. In a few cases we also selected CMEs followed by shocks at 1 AU slightly later than 4 days. The drag-based model was used to identify the definite CME-shock pairs as explained in Section 2. We found 130 CMEs driving IP shocks at 1 AU. We then investigated the particle intensities to establish ESP association. In 14 shock pas-

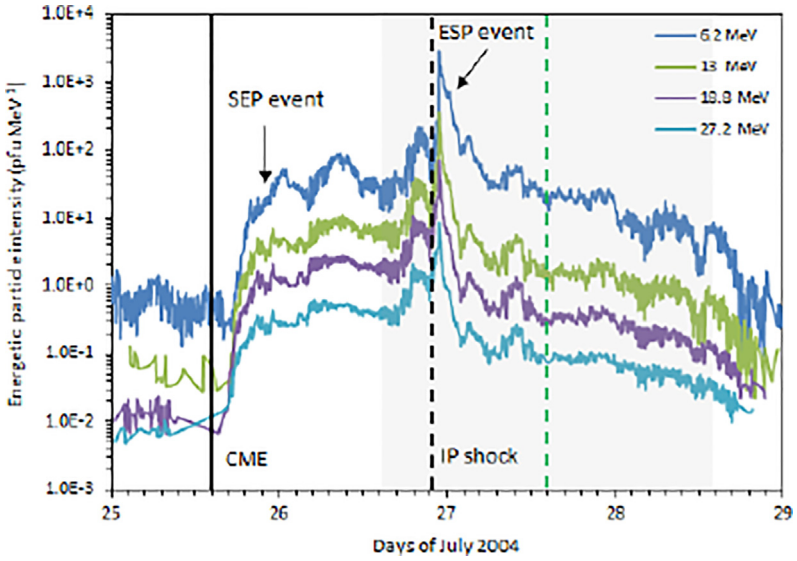

Fig. 1. Proton intensities provided by the SEPEM server as function of time during the CME-driven shock launched on July 25, 2004. The nominal proton energies from top to bottom are 6.2,13, 18.8, and 27.2 MeV. The solid black line is the launch time of the CME from the Sun and the dashed green line its predicted arrival time at 1 AU. The shaded area represents the ±24 hour time window centered on the predicted arrival time of the ICME. The dashed black line is the observed time of the interplanetary shock.

sages large fluctuations in particle intensities prevented a reliable judgement whether an ESP component was present or not. These 14 events were not included in further analysis. Sixty-six of the remaining 116 events (57%) were identified as ESP events, while 50 (43%) shocks did not have associated ESPs.

All shocks associated with ESPs were fast forward shocks. Furthermore, 45 of the 50 (90%) shocks not associated with ESPs were fast forward shocks. Of the rest, three were slow forward and two fast reverse shocks.

We estimated the maximum energy at which an ESP event was observed. All ESP events (66 events) were observed at 6.2 MeV nominal energy. At higher nominal energies the number of events were 61 (92%) at 9 MeV, 51 (77%) at 13 MeV, 42 (64%) at 18.8 MeV, 24 (36%) at 27.2 MeV, 14 (21%) at 39.3 MeV, 7 (11%) at 56.9 MeV, 3 (5%) at 82.1 MeV, and 1 (2%) at 118.9 MeV.

Type II radio bursts were associated with 88% of the CMEs with an ESP event and 54% of the CMEs without an ESP event. SEP events were associated with 77% of the CMEs with an ESP event whereas only 28% of the CMEs without an ESP event were associated with SEPs. The SEP events were associated with 51/66 (77%), 38/51 (75%), 30/42 (71%), and 17/24 (71%) of the ESP events at energies 6.2, 13.0, 18.8, and 27.2 MeV, respectively.

3.2. Characteristics of IP shocks and solar events

3.2.1. Transit speeds of IP shocks

Shock transit speed (V_{TR}) represents the mean speed of the transport of a shock in IP space from the Sun to 1 AU. We estimated V_{TR} by using the following formula:

$$V_{TR} = \frac{1AU}{T_{sh}} \quad (1)$$

The transit time of an IP shock (T_{sh}) is defined as the time from the CME launch (onset time) at the Sun to the observed IP shock time at 1 AU. The shock transit times for our sample extend from 1.18 days to 4.32 days. Fig. 2a shows the distribution of the transit speeds for shocks with (black bins) and without (gray bins) an ESP event. The bin widths in Fig. 2a are 100 km $s^{-1}$and each bin includes the events with the speed greater than or equal to the bin value but smaller than the next larger bin value. The transit speeds of the shocks with an ESP event extend from 510 km $s^{-1}$to 1468 km $s^{-1}$with the maximum in the distribution at the bin 800 km s^{-1}. For shocks without an ESP event the transit speeds of most of the shocks are in the range of 400–800 km s^{-1}. On average, the transit speeds of the shocks with an ESP event were significantly (p-value = 4.4×10^{-11}) greater than those of the shocks without an ESP event as shown in Table 1.

3.2.2. Shock parameters at 1 AU

The shock speed (V_{sh}), Alfvénic Mach number (M_A), magnetosonic Mach number (M_{ms}), shock compression ratio (CR_{sh}), and shock normal angle (θ_{bn}) are the most important parameters describing the shock properties at 1 AU. The distributions of these parameters for shocks with (black bins) and without (gray bins) an ESP event are presented in Fig. 2b-f.

The range of the shock speeds for all events was from 222 km $s^{-1}$to 1086 km $s^{-1}$with an average of 572 ± 17 km s^{-1}. The distributions of the shock speeds in Fig. 2b show that most of the shocks with an ESP event have speeds >400 km $s^{-1}$with only 4 shocks at speeds

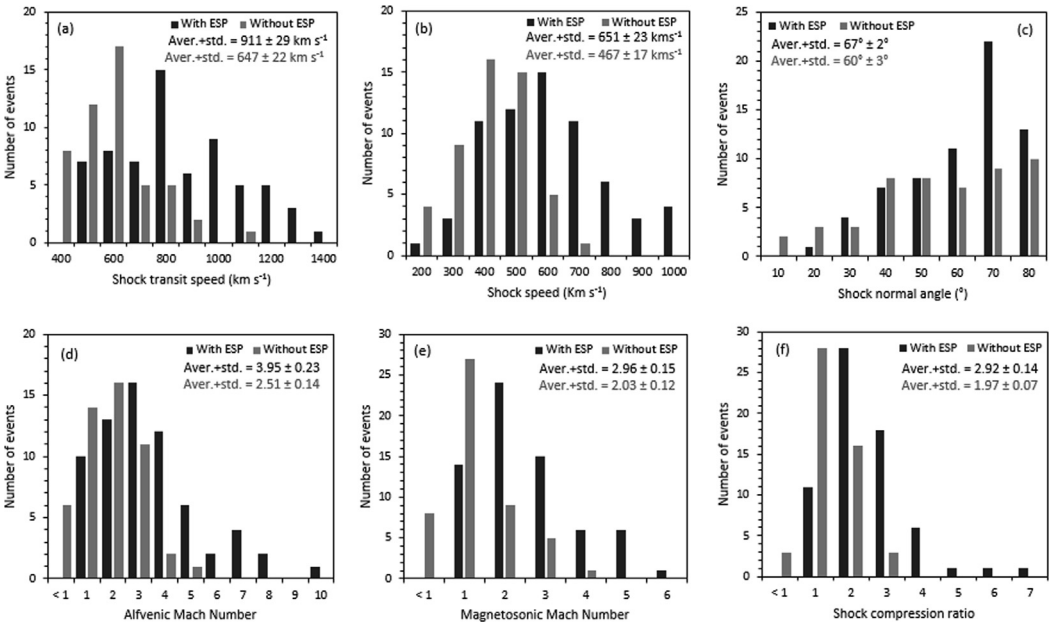

Fig. 2. The distributions of the shock transit speed, shock speed, normal angle, Alfvénic Mach number, magnetosonic Mach number, and compression ratio at 1 AU for IP shocks driven by CMEs with (black bins) and without (gray bins) ESP events. The averages with standard deviations are shown in the panels. The bin-widths are 100 km s^{-1}in panels (a) and (b), 10° in panel (c) and 1.0 units in panels (d)–(f).

Table 1
Average values with standard errors of parameters characterizing the IP shocks, CMEs, type II radio bursts and SEP events in the two groups.

Parameter	With ESP event	Without ESP event	P-value
Shock transit speed (km s^{-1})	911 ± 29	647 ± 22	4.4×10^{-11}
Shock speed (km s^{-1})	651 ± 23	467 ± 17	2.3×10^{-9}
Alfvénic Mach number	3.95 ± 0.23	2.51 ± 0.14	8.1×10^{-7}
Magnetosonic Mach number	2.96 ± 0.15	2.03 ± 0.12	5.7×10^{-6}
Shock compression ratio	2.92 ± 0.14	1.97 ± 0.07	3.5×10^{-8}
Shock normal angle (°)	67 ± 2	60 ± 3	0.047
CME linear speed (kms^{-1})	1390 ± 63	913 ± 67	1.0×10^{-6}
Halo CMEs	89%	70%	...
Angular width of partial CMEs (°)	221 ± 20	188 ± 13	0.21
Solar longitude of western CMEs (°)	38 ± 4	36 ± 6	0.79
Solar longitude of eastern CMEs (°)	−25 ± 4	−33 ± 5	0.25
Metric type II bursts	62%	44%	...
Metric type II duration (min)	9 ± 1	12 ± 1	0.12
Metric type II starting frequency (MHz)	104 ± 9	108 ± 18	0.86
DH type II bursts	86%	40%	...
DH type II duration (h)	20.9 ± 2.0	3.9 ± 1.3	5.7×10^{-10}
DH type II lowest frequency (MHz)	0.62 ± 0.24	1.46 ± 0.36	0.061
SEP events	77%	28%	...
SEP peak intensity at 6.2 MeV (pfu MeV^{-1})	137 ± 24	20.4 ± 9.3	2×10^{-5}

<400 kms^{-1}. The maximum of the distribution is at 600 kms^{-1}. On the other hand, most of the shocks without an ESP event have speeds <600 km$s^{-1}$and the maximum of the distribution is at 400 kms^{-1}. The average speed of the shocks with an ESP event (651 ± 23kms^{-1}) was significantly (p-value $\sim 10^{-9}$) higher than that of the shocks without an ESP event (467 ± 17kms^{-1}).

The distributions of M_A and M_{ms} are presented in Fig. 2d and e, respectively. The range of M_A for shocks with an ESP event was from 1.3 to 10 with a maximum at 3.0 whereas most of the shocks without an ESP event had M_A <4.0 and maximum at 2.0. The range of M_{ms} for shocks with an ESP event was from 1.11 to 6.0 with a maximum at 2.0 whereas for shocks without an ESP event the range was from 0.068 to 4.85 with a maximum at 1.0. Few shocks without an ESP event had M_A and M_{ms}< 1, while no shocks with an ESP event were found with Mach numbers <1. Note that Mach number values less than 1 for fast mode shocks are not physical and these values reflect the uncertainties in the determination of interplanetary shock parameters. Therefore, Mach numbers less than one were not included in the analyses. On average M_A and M_{ms} for

shocks with an ESP event were significantly (p-value $\sim 10^{-6}$) higher than for shocks without an ESP event as shown in Table 1.

Most of the shock compression ratios were in the range of 1.0–4.0 with a few shocks without an ESP event <1 and few with an ESP event >4 as shown in Fig. 2f. $CR_{sh}<1$ are also not physical and were not included in the analyses. The distribution of CR_{sh} for the shocks with an ESP event has a maximum at 2.0, while for the shocks without an ESP it is at 1.0. On average the CR_{sh} for the shocks with an ESP event (2.92 ± 0.14) was significantly (p-value $\sim 10^{-8}$) higher than that of the shocks without an ESP events (1.97 ± 0.07). The distribution of θ_{bn} shows a clear peak at 70° for the shocks with an ESP event, while most of the shocks without an ESP event are almost uniformly distributed within the range 40°– 80°(Fig. 2c). On average θ_{bn} for shocks with and without ESPs are similar.

3.2.3. CME characteristics at the sun

The CME characteristics at the Sun can affect the ability of the related IP shocks to accelerate particles at 1 AU. The CME linear speed (V_{CME}^{linear}), angular width, and solar longitude were used to describe the CMEs at the Sun. The distribution of V_{CME}^{linear} related to the identified IP shocks is presented in Fig. 3a. The range of V_{CME}^{linear} in ESP events was from 501 to 2861 $km\,s^{-1}$, while for events without ESPs it was 408 to 2285 $km\,s^{-1}$. As expected, the average linear CME speed for ESP events ($1390 \pm 63\,km\ s^{-1}$) was significantly higher than for the events without an ESP component ($913 \pm 67\,km\ s^{-1}$). Fifty-nine out of 66 (89%) CMEs associated with ESP events were halo CMEs. For non-ESP events the percentage was 70% (35 out of 50). The widths of the partial halo CMEs were similar for the two groups ($221° \pm 20°$ for ESP events and $188° \pm 13°$ for non-ESP events). For both groups of events the solar longitudes of the CME launch sites covered the whole longitude range of +90° to −90°. For events associated with ESPs 43 out of 66 (65%) CMEs were launched from the western hemisphere compared to 23 out of 50 (46%) for non-ESP events. There were no significant differences in the longitudes of the western CMEs ($38° \pm 4°$ vs. $36° \pm 6°$) or the eastern CMEs ($-25° \pm 4°$ vs. $-33° \pm 5°$) for the two groups of events.

3.2.4. Type II radio bursts

Solar radio type II bursts can play an important role in describing the strength of a shock producing an ESP event at 1 AU. Type II bursts were associated with 88% of the ESP events and 54% of the non-ESP events. To study the characteristics and to compare the associations of type II bursts in metric and hectometric wavelengths with ESP events, we investigated m and DH type II bursts separately. We found that 62% of events with an ESP event and 44% of events without an ESP event were related to m type II bursts. The average starting frequency and duration of the fundamental lane of m type II bursts were similar for the two groups of events as shown in Table 1. DH type II bursts were associated with 86% of the ESP events while only 40% of events without ESPs were associated with DH type II bursts. The times, frequencies, and solar sources of the associated CMEs of our DH type II bursts are in agreement with the list of Gopalswamy et al. (2019). The distributions of DH type II end frequencies and durations are presented in Fig. 3b and c, respectively. For most of the DH type II bursts related to CME-driven shocks with an ESP event (47 out of 56), the end frequencies were in the range 0.01–0.4 MHz. In nine events the end frequency was $\geqslant 0.5$ MHz. For all events without an ESP event, the end frequencies were $\geqslant 0.1$ MHz. We also found that the DH type II durations for the CME-driven shocks without an ESP event were short (<9 h) with the exception of one event with duration of 25.5 h. For the events with ESPs the durations were from 0.1 h to 49.7 h. On average the durations of DH type II bursts for events with ESPs (20.9 ± 2.0 h) were significantly (p-value $\sim 10^{-10}$) longer than for events without an ESP event (3.9 ± 1.3 h). We also investigated the ESP peak intensities at 6.2 MeV for events with and without m and DH type II bursts. The average ESP intensity for events with DH type II association (662 ± 209 pfu MeV^{-1}) was significantly ($p = 0.003$) higher than for events without DH type II bursts (23 ± 6 pfu MeV^{-1}). For events with and without m type II bursts the average intensities were similar (588 ± 263 pfu $MeV^{-1}$and 554 ± 220 pfu MeV^{-1}, respectively).

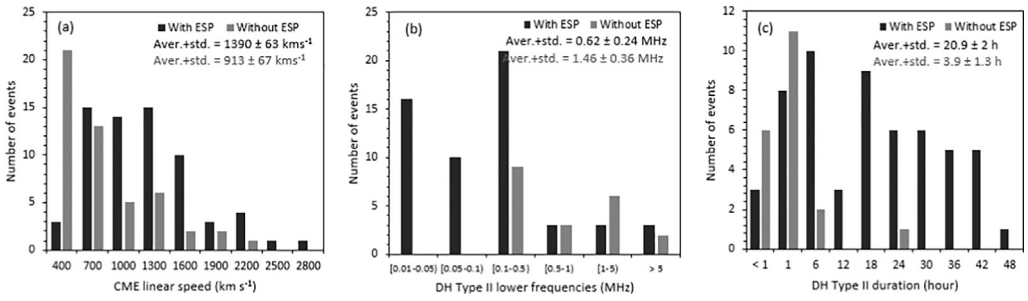

Fig. 3. The distribution of the CME linear speeds, lowest frequencies, and durations of DH type II bursts for IP shocks driven by CMEs with (black bins) and without (gray bins) ESP events. The averages with standard deviations are shown in the panels. The bin-widths are 300 $km\,s^{-1}$in panel (a) and 6 h in panel (c).

3.2.5. Solar energetic particle events

In the investigation of SEP events we found that they were associated with 51 out of 66 (77%) ESP events while SEPs were associated with only 14 out of 50 (28%) CME-driven IP shocks without ESPs. We also found that the average peak intensity of SEP protons at 6.2 MeV associated with ESP events (137 ± 24 pfu MeV^{-1}) was significantly ($p = 2 \times 10^{-5}$) higher than that of the events without ESPs (20.4 ± 9.3 pfu MeV^{-1}). On the other hand, when we compared the ESP peak intensities at 6.2 MeV for events with and without an SEP event, we found that the average ESP peak intensity in association with an SEP event (835 ± 252 pfu MeV^{-1}) was significantly ($p = 0.01$) higher than that of the events without an SEP event (130 ± 39 pfu MeV^{-1}).

3.3. Correlation analysis

We carried out correlation studies of the logarithm of the ESP peak intensities ($\log_{10}(I_{ESP}^{peak})$) with various parameters describing the IP shocks, CMEs, and SEP events. In each case, we used four proton energy ranges: 5.0–7.2 MeV (nominal energy 6.2 MeV), 10.5–15.1 MeV (13.0 MeV), 15.1–21.9 (18.8 MeV), and 21.9–31.6 MeV (27.2 MeV) provided by the SEPEM server. We estimated the Pearson correlation coefficients and their uncertainties by using the bootstrapping method of resampling with replacement. In this method samples are chosen at random from the original data. Each sample has the same size as the original, but replacement means that the same data point may be selected many times or left unselected in a sample. The random selection was repeated 1000 times, with the correlation coefficient determined for each sample. The given correlation coefficient is the average of those 1000 samples, with the standard deviation of the derived distribution representing the uncertainty. We also took into account the effect of the uncertainties in the data on the correlation coefficients. The estimated uncertainties of the data points were assumed to represent Gaussian one-sigma uncertainties. The correlation coefficients were estimated by randomly altering the data points according to a Gaussian distribution with the most likely value equal to the observed value and the standard deviation equal to each point's uncertainty. The correlation coefficient was calculated for each sample once again, and the average value and standard deviation of the distribution obtained after 1000 repetitions represent the estimated correlation coefficient and its uncertainty. Table 2 presents the Pearson correlation coefficients with their uncertainties for each parameter in the four energy ranges. Also given are the p-values, based on Student's t-test, associated with the correlation coefficients.

At each energy of 6.2, 13.0, 18.8, and 27.2 MeV there were respectively 66, 51, 42, and 24 events for which all IP shock parameters were known. We found strong correlations between $\log_{10}(I_{ESP}^{peak})$ and shock transit speeds at each energy with very low p-values as shown in Table 2. The correlation coefficients at 6.2, 13.0, 18.8, and 27.2 MeV were 0.73 ± 0.04, 0.65 ± 0.04, 0.64 ± 0.05, and 0.61 ± 0.07, respectively. We also found strong to moderate correlations between $\log_{10}(I_{ESP}^{peak})$ and V_{sh} with correlation coefficients 0.62 ± 0.05 at 6.2 MeV, 0.51 ± 0.05 at 13.0 MeV, 0.45 ± 0.06 at 18.8 MeV, and 0.44 ± 0.08 at 27.2 MeV. Fig. 4 shows the scatter plots of $\log_{10}(I_{ESP}^{peak})$ as function of V_{TR}(upper panels) and V_{sh}(lower panels) at 6.2, 13.0, and 18.8 MeV. Most of the data points of the relationship of $\log_{10}(I_{ESP}^{peak})$ with both T_{sh} and V_{sh} are closely around the linear regression lines at 6.2 MeV, but at higher energies there is a larger scatter of the data points as shown in Fig. 4. The correlation coefficients are decreasing with increasing energy of the observed ESP events.

In the investigation of the dependence of $\log_{10}(I_{ESP}^{peak})$ on M_A and M_{ms}, we found only weak to moderate correlations. The correlation coefficients were highest at 27.2 MeV (0.59 ± 0.10 and 0.55 ± 0.12, for M_A and M_{ms} respectively) while lower correlations were found at 6.2 MeV (0.26 ± 0.06 and 0.26 ± 0.07). The scatter plots of $\log_{10}(I_{ESP}^{peak})$ as function of M_A and M_{ms} at 6.2, 18.8, and 27.2 MeV are shown in Fig. 5. The $\log_{10}(I_{ESP}^{peak})$ were also found to be weakly correlated with $CR_{sh}$with the p-value about 0.05. The highest correlation (0.33 ± 0.12) was found at 27.2 MeV. No significant correlations were found between $\log_{10}(I_{ESP}^{peak})$ and θ_{bn}.

The dependence of $\log_{10}(I_{ESP}^{peak})$ on the CME parameters was also investigated. The CME linear speed (V_{CME}^{linear}) and space speed (V_{CME}^{space}), the solar connection angle ($\Delta\phi$), and the angular distance from the disk center (α) were used as CME parameters. We use the space speeds only for the halo CMEs (59 out of 66) as given in the CDAW halo CME list (Gopalswamy et al., 2010b). We found weak to moderate correlations between $\log_{10}(I_{ESP}^{peak})$ and V_{CME}^{linear} and V_{CME}^{space}. The correlations were highest at 18.8 MeV (0.50 ± 0.04 and 0.51 ± 0.04, respectively). All correlation coefficients are presented in Table 2. The scatter plots of $\log_{10}(I_{ESP}^{peak})$ as function of CME linear speed at 6.2, 13.0, and 18.8 MeV are presented in Fig. 6 (upper panels).

The solar connection angle is defined as the longitudinal distance ($\triangle\phi$) of the flare from the footpoint of the Parker spiral leading to the spacecraft near 1 AU. The longitudinal distance was estimated using the following formula:

$$\triangle\phi = \phi_{fl} - \frac{\Omega_{\odot} r_{s/c}}{u_{sw}} \quad (2)$$

where ϕ_{fl} is the solar flare longitude, $2\pi\Omega_{\odot}^{-1} = 24.47d$ is the equatorial period of the solar rotation, $r_{s/c}$ is the radial distance of the spacecraft from the Sun, and u_{sw} is the average solar wind speed. The solar wind speed was observed by the SOHO spacecraft and averaged over the period of five hours centered at the hour of the ESP peak time. The solar connection angle is positive for flares to the west from the footpoint and negative for flares to the east. The connec-

Table 2
Correlation coefficients at four energy channels between the logarithm of peak intensities of ESP events and various IP shock and CME parameters, and SEP peak intensities. The p-value of the null-hypothesis that there is no correlation between the variables is given in parentheses under each coefficient.

Parameter	6.2 MeV	13 MeV	18.8 MeV	27.2 MeV
Shock transit speed	0.73 ± 0.04 ($< 10^{-4}$)	0.65 ± 0.04 ($< 10^{-4}$)	0.64 ± 0.05 ($< 10^{-4}$)	0.61 ± 0.07 ($< 10^{-3}$)
Shock speed	0.62 ± 0.05 ($< 10^{-4}$)	0.51 ± 0.05 ($< 10^{-4}$)	0.45 ± 0.06 (0.0014)	0.44 ± 0.08 (0.016)
Alfvénic Mach number	0.26 ± 0.06 (0.018)	0.46 ± 0.07 ($< 10^{-3}$)	0.47 ± 0.07 ($< 10^{-3}$)	0.59 ± 0.10 (0.0012)
Magnetosonic Mach number	0.26 ± 0.07 (0.018)	0.40 ± 0.08 (0.0018)	0.40 ± 0.09 (0.0043)	0.55 ± 0.12 (0.0027)
Compression ratio	0.20 ± 0.09 (0.054)	0.23 ± 0.09 (0.052)	0.24 ± 0.11 (0.063)	0.33 ± 0.12 (0.057)
Shock normal angle	0.05 ± 0.07 (0.35)	0.02 ± 0.08 (0.44)	0.10 ± 0.09 (0.26)	0.10 ± 0.10 (0.32)
CME linear speed	0.37 ± 0.04 (0.001)	0.44 ± 0.04 ($< 10^{-3}$)	0.50 ± 0.04 ($< 10^{-3}$)	0.47 ± 0.06 (0.01)
CME space speed	0.47 ± 0.04 ($< 10^{-4}$)	0.49 ± 0.04 ($< 10^{-3}$)	0.51 ± 0.04 ($< 10^{-3}$)	0.46 ± 0.06 (0.016)
Connection angle	0.13 ± 0.02 (0.15)	0.27 ± 0.02 (0.028)	0.39 ± 0.02 (0.006)	0.11 ± 0.03 (0.3)
Angular distance	−0.21 ± 0.03 (0.044)	−0.15 ± 0.03 (0.14)	−0.01 ± 0.03 (0.47)	−0.01 ± 0.04 (0.48)
SEP peak intensity	0.44 ± 0.04 ($< 10^{-3}$)	0.55 ± 0.03 ($< 10^{-4}$)	0.57 ± 0.03 ($< 10^{-4}$)	0.61 ± 0.03 (0.0046)

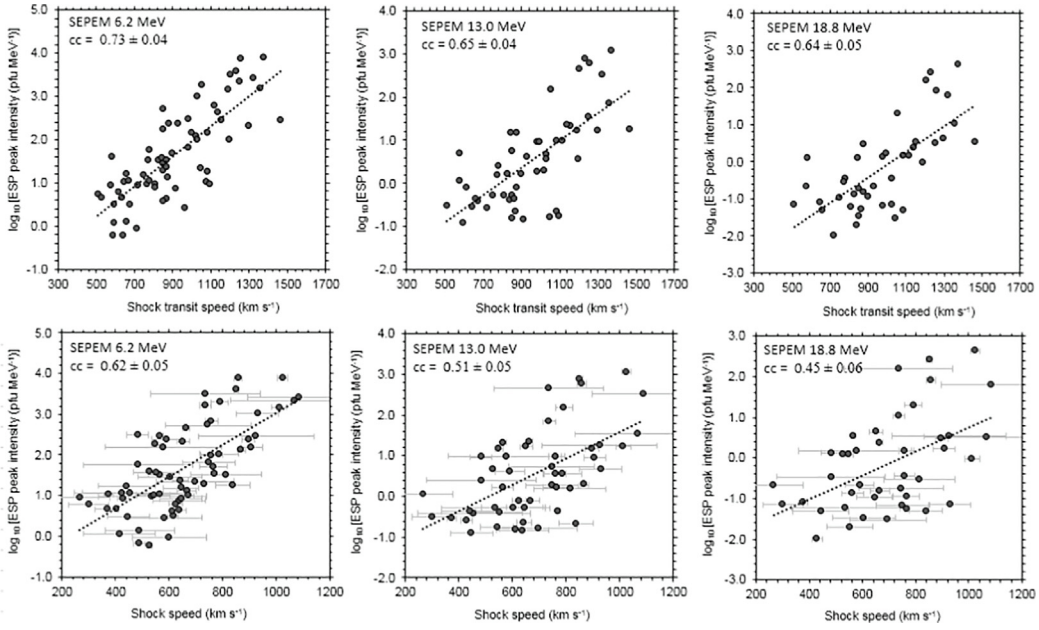

Fig. 4. Scatter plots of the logarithm of the ESP peak intensities as function of the shock transit speeds (upper panels) and shock speeds (lower panels) at 6.2, 13.0, and 18.8 MeV. The best-fit linear regression lines are shown by the black dotted lines. The error bars of the data points indicate the uncertainties in the estimated shock speeds. The calculated correlation coefficients with their standard deviations are shown in the panels.

tion angle for the ESP event on September 25, 2011 (−164) was discarded from the analysis as an outlier. The highest correlation coefficient of 0.39 ± 0.02 (p-value = 0.006) between $\log_{10}(I_{ESP}^{peak})$ and $\Delta\phi$ was found at 18.8 MeV. However, at 27.2 MeV there was no significant correlation. Also at lowest energies the correlation was weak (see Table 2). The scatter plots of $\log_{10}(I_{ESP}^{peak})$ as function of $\Delta\phi$ at 6.2, 18.8, and 18.8 MeV are shown in Fig. 6 (lower panels). For the relationship between $\log_{10}(I_{ESP}^{peak})$ and α we found a negative weak correlation (−0.21 ± 0.03) at 6.2 MeV with p-value of 0.044 and no significant correlation was found at higher energy ranges as presented in Table 2.

Finally, we investigated the relationship between the ESP peak intensities at 1 AU and the SEP peak intensities.

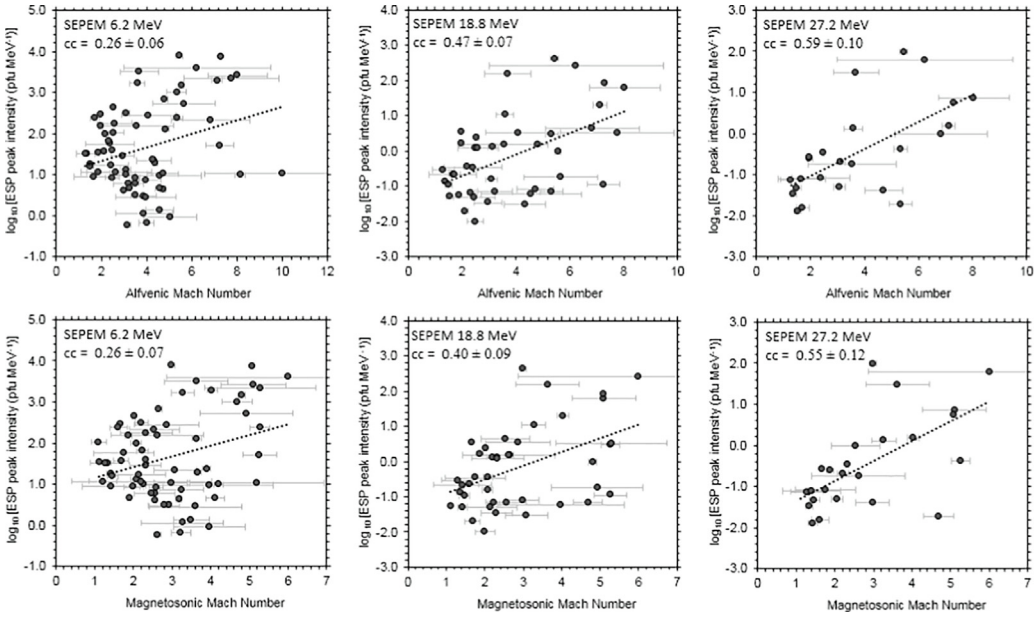

Fig. 5. Scatter plots of the logarithm of ESP peak intensities as function of Alfvénic (upper panels) and magnetosonic (lower panels) Mach numbers at 6.2, 18.8, and 27.2 MeV. The best-fit linear regression lines are shown by the black dotted lines. The error bars of the data points indicate the uncertainties in the estimated Mach numbers. The calculated correlation coefficients with their standard deviations are shown in the panels.

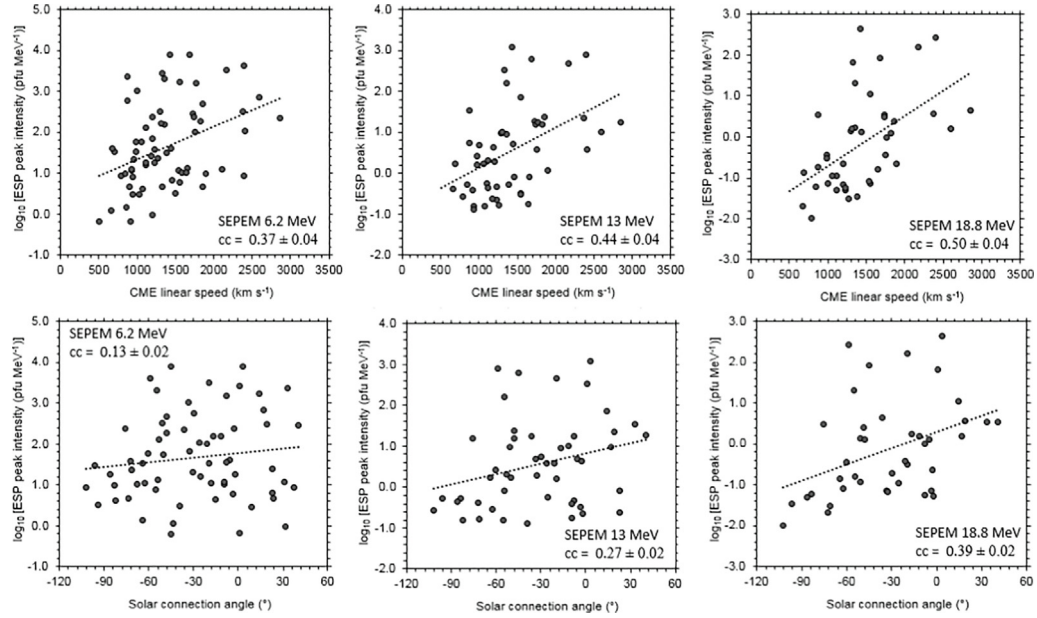

Fig. 6. Scatter plots of the logarithm of ESP peak intensities as function of CME linear speed (upper panels) and solar connection angle (lower panels) at 6.2, 13.0, and 18.8 MeV. The best-fit linear regression lines are shown by the black dotted lines. The calculated correlation coefficients with their standard deviations are shown in the panels.

SEPs are accelerated at or close to the Sun and are identified as the significantly earlier rise of the particle intensities compared to ESPs. We found that the correlation between $\log_{10}(I_{SEP}^{peak})$ and $\log_{10}(I_{ESP}^{peak})$ was energy dependent: highest at 27.2 MeV (0.61 ± 0.03) and lowest at 6.2 MeV (0.44 ± 0.04). Fig. 7 shows the scatter plots of $\log_{10}(I_{SEP}^{peak})$ as function of $\log_{10}(I_{ESP}^{peak})$ at 6.2, 13.0, and 27.2 MeV.

3.4. Dependence between shock parameters at 1 AU, shock transit speed, and CME speed

In Section 3.3 we showed that the shock parameters at 1 AU that have the highest correlation coefficients with the ESP maximum intensity were the shock speed and Mach numbers. We further investigated the dependence of these shock parameters (V_{sh}, M_A, and M_{ms}) at 1 AU on

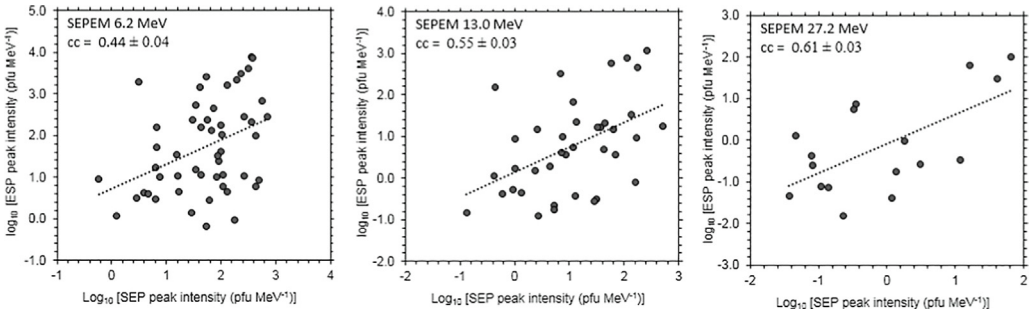

Fig. 7. Scatter plots of the logarithm of ESP peak intensities as function of the logarithm of SEP peak intensities at 6.2, 13.0, and 27.2 MeV. The best-fit linear regression lines are shown by the black dotted lines. The calculated correlation coefficients with their standard deviations are shown in the panels.

V_{CME}^{linear} and V_{TR}. First, we found that the shock transit speed was only weakly dependent on V_{CME}^{linear} with correlation coefficient of 0.34 ± 0.05 as shown in Fig. 8a. This dependence was also similar for shocks with and without ESP association. This indicates that the transport of a CME-driven shock in IP space from the Sun to 1 AU may experience different levels of acceleration or deceleration. The shock parameters V_{sh}, M_A, and M_{ms} were not significantly correlated with V_{CME}^{linear}. The correlation coefficients were 0.12 ± 0.05, 0.02 ± 0.07, and -0.08 ± 0.09, respectively (see Fig. 8b for V_{sh} vs. V_{CME}^{linear}). On the other hand we found that V_{sh} was strongly dependent on V_{TR} with correlation coefficient of 0.66 ± 0.05 (p-value $<10^{-4}$) as shown in Fig. 8c. The Mach numbers M_A and M_{ms} had a weak correlation with V_{TR}(0.31 ± 0.05 and 0.23 ± 0.06) and V_{sh}(0.31 ± 0.08 and 0.32 ± 0.08).

4. Summary and discussion

We have investigated the occurrence and relationships of high-energy ESP events with several parameters that describe interplanetary shocks driven by CMEs at 1 AU and the associated CMEs, solar type II radio bursts and SEP events. We analysed 116 IP shocks driven by front-side full and partial halo CMEs with speed $>400\,\mathrm{km\,s^{-1}}$ and their associations with high-energy protons during the time period 1996–2015. Based on the time-intensity profiles of protons at energies >1 MeV observed by SOHO/ERNE or found in the data provided by the SEPEM server, we identified 66 out of the 116 (57%) IP shocks to be associated with an ESP event observed during the shock passage. For 50 (43%) IP shocks we did not find an enhancement of the proton intensity related to the shock passage. For fast forward shocks driven by CMEs, Ho et al. (2008) found that 64% and 32% of the shocks were associated with an ion flux enhancement at 47–68 keV and 1.9–4.8 MeV, respectively. Mäkelä et al. (2011) reported that 75% of their selected shocks had an ESP signature in the proton intensity observed at 0.11–0.19 keV, while at 1.9–4.8 MeV the percentage had dropped to 45%. Huttunen-Heikinmaa and Valtonen (2009) found that 46% of fast forward shocks, irrespective of their origins, did not show any signs of an ESP event. The differences in these results can most probably be explained by different event selection criteria.

4.1. Occurrence of ESP events

The occurrence of ESP events is dependent on the transit speed (V_{TR}) of IP shocks from the Sun to 1 AU. The distribution of V_{TR} in Fig. 2a shows a bi-modal structure with a maximum at 800 km $s^{-1}$for shocks with an ESP event and 600 km $s^{-1}$for shocks without an ESP signature. The shocks with an ESP event had transit speeds >700 km s^{-1}- in 77% of the cases, while 74% of the shocks without an ESP event had transit speeds <700 km s^{-1}. On average the transit speed of shocks with an ESP event (911 ±

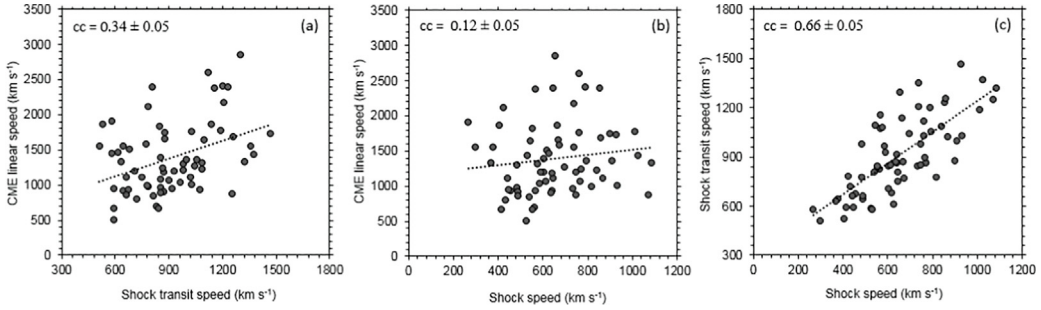

Fig. 8. (a) Scatter plots of the CME linear speed as function of the shock transit speed, (b) the CME speed as function of the shock speed at 1 AU, and (c) the shock transit speed as function of the shock speed at 1 AU. The best-fit linear regression lines are shown by the black dotted lines. The calculated correlation coefficients with their standard deviations are shown in the panels.

29 km s^{-1}) was significantly higher than of shocks without an ESP event ((647 ± 22 km s^{-1}). Thus, the shocks with faster transit speeds seem to be more frequently capable to accelerate particles at 1 AU compared to shocks with slower transit speeds.

The distributions of the parameters V_{sh}, M_A, M_{ms}, CR_{sh}, and θ_{bn} with and without an ESP event were significantly overlapping (Fig. 2 b-f). However, on average all shock parameters, with an exception of the shock normal angle, had significantly greater values in shocks associated with an ESP event compared to those without an ESP event (Table 1). The average M_A of shocks with an ESP event is 1.57 times higher than that of shocks without an ESP event. For the other parameters the difference is somewhat smaller (1.46 for M_{ms}, 1.48 for CR_{sh}, and 1.4 for V_{sh}). The average shock normal angle between the two groups showed an insignificant difference, but we note that the distribution of shock normal angles for ESP events has a peak around 70°, which is missing from the distribution of shocks without an ESP event. The characteristics of IP shocks at 1 AU play an important role in producing ESP events. As expected, our results show that IP shocks that produce an ESP event have greater strength than those that do not.

The distributions of linear speeds, angular widths, and solar longitudes of CMEs associated with IP shocks with and without an ESP event were significantly overlapping (see Fig. 3 a for V_{CME}^{linear}). The averages of the angular widths and solar longitudes of CMEs were similar for shocks with and without an ESP event. However the average of CME linear speeds related to shocks with an ESP event (1390 ± 63 km s^{-1}) was significantly higher than for shocks without an ESP event (913 ± 67 km s^{-1}). Our findings are in agreement with the results reported by Mäkelä et al. (2011). They found that the average of M_A(3.46), and CME speed (1088 km s^{-1}) for shocks accelerating ESPs were significantly higher than for shocks without an ESP event (2.22, 771 km s^{-1}, respectively).

Type II radio bursts were associated with 88% and 54% of the CME-driven shocks with and without an ESP event respectively. Mäkelä et al. (2011) found that 52% of radio-loud (RL) shocks and only 33% of radio-quiet (RQ) shocks produced an ESP event at proton energies >1 MeV. In our study, 67% of RL shocks and 27% of RQ shocks were associated with ESP events. Thus, full and partial halo CME-driven RL shocks are significantly more likely associated with an ESP event than RQ shocks. We further studied the associations and properties of m and DH type II radio bursts separately. Metric type II bursts were associated with 62% of shocks with an ESP event and 44% of shocks without an ESP event. The starting frequencies and the durations of the fundamental lane of m type II were similar for the two groups. At DH wavelengths we found that 86% of shocks with an ESP event were associated with DH type II bursts whereas only 40% of shocks without ESPs had this association. On average the end frequency (0.62 ± 0.24 MHz) was significantly lower and the duration (20.9 ± 2.0 h) longer for DH type II bursts associated with shocks with an ESP event compared to shocks without an ESP event (1.46 ± 0.36 MHz and 3.9 ± 1.3 h, respectively). We also found that the average ESP intensity at 6.2 MeV for events associated with DH type II burst was significantly higher than that of events without DH type II burst. Gopalswamy et al. (2019) found a significant difference between the lowest frequencies of DH type II bursts in solar cycles 23 and 24. Solar cycle dependence was visible also in our DH type II bursts, but the average maximum intensities of the associated ESP events were similar for the two solar cycles.

When investigating associations between ESP and SEP events, we found that 77% of shocks with an ESP event were associated with an SEP event whereas only 28% of shocks without ESPs were associated with an SEP event. In another way, 79% of CME-driven shocks associated with an SEP event were also associated with an ESP event at 1 AU whereas 29% of CME-driven shocks without an SEP event produced an ESP event. On average the SEP peak intensity at 6.2 MeV associated with IP shocks that produced an ESP event was significantly higher than for shocks without an ESP event. Also the average ESP peak intensity at 6.2 MeV for events associated with SEPs was significantly higher than that of events without SEPs. Considering DH type II radio bursts and SEP events together, our results show that IP shocks driven by CMEs related to energetic (long durations and low end frequencies) DH type II bursts and high-intensity SEP events tend to produce more frequently ESP events with larger particle flux enhancements than IP shocks with weak or without DH type II burst and SEP event. It appears that DH type II bursts and SEP events could provide useful means for predicting the occurrence of ESP events at 1 AU.

4.2. ESP peak intensities

We calculated the Pearson correlation coefficients between the IP shock and solar parameters and ESP peak intensities at proton energies 6.2, 13.0, 18.8, and 27.2 MeV. The highest correlation coefficient was found between $\log_{10}(I_{ESP}^{peak})$ and V_{TR} at 6.2 MeV (0.73 ± 0.04) while at higher energies the correlation was decreasing. According to our knowledge the relation between ESP peak intensities and shock transit speeds has not been reported previously. We conclude that the transit speeds of shocks driven by CMEs play an important role in the occurrence and intensity of ESP events at 1 AU.

Concerning the parameters describing the shocks at 1 AU, we found the highest correlation between $\log_{10}(I_{ESP}^{peak})$ and V_{sh} at 6.2 MeV (0.62 ± 0.05). Thus, the correlation with V_{sh} was strong, but still weaker than with V_{TR}. As for V_{TR}, the correlation with V_{sh} was decreasing with increasing energy as presented in Table 2. The highest correlations with M_A(0.59 ± 0.10), M_{ms}(0.55 ± 0.12) and

CR_{sh}(0.33 ± 0.12) were found at 27.2 MeV while at 6.2 MeV the correlations were lower (0.26 ± 0.06, 0.26 ± 0.07, 0.20 ± 0.09, respectively). Contrary to the correlations of V_{TR} and V_{sh}, the correlation of M_A, M_{ms} and CR_{sh}- were increasing with energy. No correlation was found between $\log_{10}(I_{ESP}^{peak})$ and θ_{bn} at any energy. Mäkelä et al. (2011) found that the correlations between the shock speed and the ESP peak intensities at proton energies 0.114–0.190 keV and 1.89–4.75 MeV were 0.59 and 0.70 respectively. Reames (2012) investigated the peak intensities of He ions at 1.65–2.00 MeV and reported the correlation coefficients of 0.81, 0.35, and 0.12 for V_{sh}, CR_{sh}, and θ_{bn}, respectively.

As expected $\log_{10}(I_{ESP}^{peak})$ showed only moderate correlations with V_{CME}^{linear} and V_{CME}^{space}(Table 2). The connection angle ($\triangle\phi$) showed very weak to moderate correlations with $\log_{10}(I_{ESP}^{peak})$ while the angular distance (α) showed weak correlations at low energies to no correlations at high energies. Mäkelä et al. (2011) found surprisingly high correlations between CME speed and ESP peak intensity at 0.114–0.190 keV (0.60) and 1.89–4.75 MeV (0.69) compared to our results.

In general our results of the dependence of the ESP peak intensities on the IP shock parameters at 1 AU and the CME linear speed are in agreement with the correlations of the SEP peak intensities with coronal shock parameters and the CME linear speed reported by Kouloumvakos et al. (2019). The coronal shock parameters were derived by 3D reconstruction techniques. Kouloumvakos et al. (2019) found strong correlations with the Mach numbers and moderate correlations with V_{CME}^{linear}, V_{sh}, and CR_{sh}- whereas θ_{bn} did not show correlation with SEP peak intensities at three proton energy ranges (20–26 MeV, 40–60 MeV, and 60–100 MeV).

In our study, the correlations between SEP and ESP peak intensities were from moderate at low (6.2 MeV) energy (0.44 ± 0.04) to strong at highest (27.2 MeV) energy (0.61 ± 0.03). Luhmann and Mann (2007) also showed that the SEP and ESP peak fluxes appeared to be correlated at proton energies near 1, 10, and 50 MeV. As mentioned in Section 4.1 the IP shocks driven by CMEs related to SEP events tend to produce more frequently ESP events. Our findings also indicate that for an SEP-ESP pair related to the same CME-driven shock the ESP maximum intensity at 1 AU is proportional to the SEP maximum intensity with the correlation increasing with energy at least up to 27.2 MeV nominal energy.

5. Conclusions

Sixty-six (57%) of the 116 IP shocks at 1 AU driven by full and partial halo CMEs with speed >400 km s^{-1}analysed in this investigation were associated with energetic storm particles at >1 MeV proton energies. In general, most of the parameters investigated indicated that shocks associated with ESPs are stronger than those without ESPs. However, the shock transit speed from the Sun to 1 AU turned out to be the parameter best distinguishing shocks capable of accelerating ESPs from those that did not have ESP association. The distribution of transit speeds of shocks with ESPs concentrates in the region above 700 km s^{-1}, while most of the shocks that did not produce ESPs had transit speeds slower than 700 km s^{-1}. The shock speed at 1 AU did not as clearly separate these two groups of shocks. The peak intensity of ESPs also more strongly depends on the shock transit speed than on the shock speed at the time of the shock passage. The correlation between ESP peak intensity and shock speed at 1 AU is what one could expect, but even stronger dependence on the shock transit speed is less obvious. An explanation could be that many shocks with slow transit speeds have already significantly weakened when reaching 1 AU, although could have been capable to accelerate particles still somewhat closer to the Sun. These would be shocks not associated with ESPs or in some cases associated with ESPs reaching the observer already slightly before the shock arrival. On the other hand, shocks with fast transit speeds have retained their strength and are therefore more often associated with ESP events.

Decametric–hectometric type II radio bursts were associated with 86% and solar energetic particles with 77% of the shocks producing ESPs, while only 40% and 28% of the shocks without ESPs had these associations. The duration of DH type II bursts was significantly longer and the end frequency significantly lower for shocks producing ESPs compared to those without ESPs. The peak intensities of SEPs and ESPs related to the same CME-driven shock were strongly correlated at high energies. Thus, DH type II radio burst and SEP observations could provide warning signals for strong ESP events.

Declaration of Competing Interest

The authors declare that they have no known competing financial interests or personal relationships that could have appeared to influence the work reported in this paper.

Acknowledgements

The authors gratefully acknowledge the various online data centers of NOAA and NASA. The LASCO CME catalog is generated and maintained by the Center for Solar Physics and Space Weather, The Catholic University of America in cooperation with the Naval Research Laboratory and NASA. Part of the data analysis for this article was generated using the Real Statistics Resource Pack software maintained by Charles Zaiontz. R.V. acknowledges funding from the European Union's Horizon 2020 research and innovation programme under grant agreement No 101004159 (SERPENTINE).

References

Berdichevsky, D.B., Szabo, A., Lepping, R.P., Viñas, A.F., Mariani, F., 2000. Interplanetary fast shocks and associated drivers observed through the 23rd solar minimum by Wind over its first 2.5 years. J. Geophys. Res. 105, 27289–27314. https://doi.org/10.1029/1999JA000367.

Brueckner, G.E., Howard, R.A., Koomen, M.J., et al., 1995. The Large Angle Spectroscopic Coronagraph (LASCO). Sol. Phys. 162, 357–402. https://doi.org/10.1007/BF00733434.

Bryant, D.A., Cline, T.L., Desai, U.D., McDonald, F.B., 1962. Explorer 12 observations of solar cosmic rays and energetic storm particles after the solar flare of September 28, 1961. J. Geophys. Res. 67, 4983–5000. https://doi.org/10.1029/JZ067i013p04983.

Cohen, C.M.S., 2006. Observations of energetic storm particles: An overview. Washington DC Am. Geophys. Union Geophys. Monograph Ser. 165, 275–282. https://doi.org/10.1029/165GM26.

Crosby, N., Heynderickx, D., Jiggens, P., Aran, A., Sanahuja, B., 2015. SEPEM: a tool for statistical modelling the solar energetic particle environment. Space Weather 13, 406–426. https://doi.org/10.1002/2013SW001008.

Dayeh, M.A., Desai, M.I., Ebert, R.W., Elliott, H., Farahat, A., Kozarev, K., Li, G., 2018. What causes the variability in the properties of energetic storm particle (ESP) events? J. Phys. Conf. Ser. 1100, 012008. https://doi.org/10.1088/1742-6596/1100/1/012008.

Dierckxsens, M., Tziotziou, K., Dalla, S., et al., 2015. 2015, Relationship between Solar Energetic Particles and Properties of Flares and CMEs: Statistical Analysis of Solar Cycle 23 Events. Sol. Phys. 290, 841–874. https://doi.org/10.1007/s11207-014-0641-4.

Ebert, R.W., Dayeh, M.A., Desai, M.I., Jian, L.K., Li, G., Mason, G.M., 2016. Multi-spacecraft analysis of energetic heavy ion and interplanetary shock properties in energetic storm particle events near 1 au. Astrophys. J. 831, 153. https://doi.org/10.3847/0004-637X/831/2/153.

Edberg, N.J.T., Lester, M., Cowley, S.W.H., Brain, D.A., Fränz, M., Barabash, S., 2010. Magnetosonic Mach number effect of the position of the bow shock at Mars in comparison to Venus. J. Geophys. Res. 115, A07203. https://doi.org/10.1029/2009JA014998.

Giacalone, J., 2012. Energetic charged particles associated with strong interplanetary shocks. Astrophys. J. 761, 1. https://doi.org/10.1088/0004-637X/761/1/28.

Gopalswamy, N., Xie, H., Mäkelä, P., Akiyama, S., Yashiro, S., Kaiser, M.L., Howard, R.A., Bougeret, J.L., 2010a. Interplanetary shocks lacking type II radio bursts. Astrophys. J. 710, 1111. https://doi.org/10.1088/0004-637X/710/2/1111.

Gopalswamy, N., Yashiro, S., Michalek, G., Xie, H., Mäkelä, P., Vourlidas, A., Howard, R.A., 2010b. A catalog of halo coronal mass ejections from SOHO. Sun Geosphere 5, 7–16, https://ui.adsabs.harvard.edu/abs/2010SunGe...5....7G.

Gopalswamy, N., Mäkelä, P., Yashiro, S., 2019. A Catalog of Type II radio bursts observed by Wind/WAVES and their statistical properties. Sun Geosphere 14, 111–121, https://ui.adsabs.harvard.edu/abs/2019SunGe.14.111G.

Ho, G.C., Lario, D., Decker, R.B., Roelof, E.C., Desai, M., Smith, C.W. 2003, Energetic electron associated with transient interplanetary shocks: Evidence for weak interaction. In: 28th International Cosmic ray conference, pp. 3689–3692. https://ui.adsabs.harvard.edu/abs/2003ICRC..6.3689H.

Ho, G.C., Lario, D., Decker, R.B., Smith, C.W., Hu, Q. 2008, Transient Shocks and Associated Energetic Particle Distributions Observed by ACE during Cycle 23, In: AIP Conference Proceeding 1039, (eds.) Li, G. et al., New York, 184. https://doi:10.1063/1.2982443.

Huttunen-Heikinmaa, K., Valtonen, E., 2009. Interplanetary fast forward shocks and energetic storm particle events above 1.5 MeV. Ann. Geophys. 27, 767–779. https://doi.org/10.5194/angeo-27-767-2009.

Jian, L., Russell, C.T., Luhmann, J.G., Skoug, R.M., 2006. Properties of Stream Interactions at One AU During 1995–2004. Sol. Phys. 239, 337–392. https://doi.org/10.1007/s11207-006-0132-3.

Kallenrode, M.B., 1995. Particle acceleration at interplanetary shocks–Observations at a few tens of keV vs some tens of MeV. Adv. Space Res. 15, 375–384. https://doi.org/10.1016/0273-1177(94)00120-P.

Kasper, J.C. 2003, Solar wind plasma: kinetic properties and micro-instabilities, Massachusetts Institute of Technology. https://ui.adsabs.harvard.edu/abs/2003PhDT....249K.

Kouloumvakos, A., Nindos, A., Valtonen, E., et al., 2015. Properties of solar energetic particle events inferred from their associated radio emission. Astron. Astrophys. 580, A80. https://doi.org/10.1051/0004-6361/201424397.

Kouloumvakos, A., Rouillard, A.P., Wu, Y., Vainio, R., et al., 2019. Connecting the properties of coronal shock waves with those of solar energetic particles. Astrophys. J. 876, 80. https://doi.org/10.3847/1538-4357/ab15d7.

Lario, D., Ho, G.C., Decker, R.B., Roelof, E.C., Desai, M.I., Smith, C. W., 2003. ACE observations of energetic particles associated with transient interplanetary shocks. AIP Conf. Proc. 679, 640–643. https://doi.org/10.1063/1.1618676.

Lario, D., Hu, Q., Ho, G.C., Decker, R.B., Roelof, E.C., Smith, C.W., 2005. Statistical properties of fast forward transient interplanetary shocks and associated energetic particle events: ACE observations. Solar Wind 11/SOHO 16, Connect. Sun Heliosphere 592, 81, https://ui.adsabs.harvard.edu/abs/2005ESASP.592...81L.

Lindsay, G.M., Russell, C.T., Luhmann, J.G., Gazis, P., 1994. On the sources of interplanetary shocks at 0.72 AU. J. Geophys. Res. 99, 11–18. https://doi.org/10.1029/93JA02666.

Luhmann, J.G., Mann, Adam, 2007. Relative fluxes of shock and prompt peaks in SEP event time profiles. Adv. Space Res. 39, 1882–1889. https://doi.org/10.1016/j.asr.2007.01.070.

Mäkelä, P., Gopalswamy, N., Akiyama, S., Xie, H., Yashiro, S., 2011. Energetic storm particle events in coronal mass ejection-driven shocks. J. Geophys. Res. (Space Phys.) 116, A08101. https://doi.org/10.1029/2011JA016683.

Rao, U.R., McCracken, K.G., Bukata, R.B., 1967. Cosmic ray propagation processes 2: The energetic storm-particle event. J. Geophys. Res. 72, 4325–4341. https://doi.org/10.1029/JZ072i017p04325.

Reames, V.D., 1999. Solar energetic particles: Is there time to hide? Radiat. Meas. 30, 297–308, https://ui.adsabs.harvard.edu/abs/1999RadM...30.297R.

Reames, V.D., 2004. Solar energetic particle variations. Adv. Space Res. 34, 381–390, https://ui.adsabs.harvard.edu/abs/2004AdSpR.34.381R.

Reames, V.D., 2012. Particle energy spectra at travelling interplanetary shock waves. Astrophys. J. 757, 93. https://doi.org/10.1088/0004-637X/757/1/93.

Sarris, E.T., Van Allen, J.A., 1974. Effects of interplanetary shock waves on energetic charged particles. J. Geophys. Res. 79, 4157–4173. https://doi.org/10.1029/JA079i028p04157.

Torsti, J., Valtonen, E., Lumme, M., et al., 1995. Energetic particle experiment (ERNE). Sol. Phys. 162, 505–531. https://doi.org/10.1007/BF00733438.

Tsurutani, B.T., Lin, R.P., 1985. Acceleration of greater than 47 keV ions and greater than 2 keV electrons by interplanetary shocks at 1 AU. J. Geophys. Res. 90, 1–11. https://doi.org/10.1029/JA090iA01p00001.

Turner, R., 2001. What we must know about solar particle events to reduce the risk to astronauts. Washington DC Am. Geophys. Union Geophys. Monograph Series 125, 39–44, https://ui.adsabs.harvard.edu/abs/2001GMS...125...39T.

Vršnak, B., Žic, T., Vrbanec, D., et al., 2013. Propagation of interplanetary coronal mass ejections: The drag-based model. Sol. Phys. 285, 295–315. https://doi.org/10.1007/s11207-012-0035-4.